Proceedings of IDETC/CIE 2005
ASME 2005 International Design Engineering Technical Conferences &
Computers and Information in Engineering Conference
September 24-28, 2005, Long Beach, California, USA

DETC2005-84482

DYNAMIC FINITE ELEMENT MODELING OF CARBON NANOTUBES USING AN INTRINSIC FORMULATION

Michael J. Leamy
The MITRE Corporation
7515 Colshire Drive
McLean, VA 22102
mjleamy@mitre.org

ABSTRACT

This article presents an efficient explicit dynamic formulation for modeling curved and twisted Carbon Nanotubes (CNT's) based on a recently-developed *intrinsic* beam description (i.e. the dynamic state given by curvatures, strains, and velocities only) [Hodges, 2003] together with a finite element discretization incorporating atomistic potentials. This approach offers several advantages primarily related to the model's computational efficiency: 1) the resulting partial differential equations governing motion are in first-order form (i.e. have first-order time derivatives only), 2) the system nonlinearities appear at low order, 3) the intrinsic description incorporating curvature allows low-order interpolation functions to describe generally curved and twisted nanotube centerlines, 4) inter-element displacements, slopes, and curvatures are matched at the element boundaries, and 5) finite rotational variables are absent, along with their inherit complexities. In addition, the developed model and finite element discretization are able to capture the nanotube's dynamic response, without the expense of calculating the dynamic response of individual atoms as per Molecular Dynamics models. Simulation results are presented which illustrate the dynamic response of a typical CNT to axial, bending, and torsional loading. Results from the simulations are compared to similar results available in the literature, and close agreement is documented. Keywords: nanotube, nanomaterial, finite element, dynamic, computational nanomechanics

1. INTRODUCTION

The intent of this study is to develop a computationally efficient, dynamic, model of a carbon nanotube (CNT) for later incorporation into a general framework capable of simulating *CNT nanocomposites*, i.e. composite materials composed of a matrix material reinforced by fiber-like carbon nanotubes. It is anticipated that nanocomposites may be used in diverse applications where the geometry and loading may not be of a simplistic nature. It is also anticipated that a large-degree of accuracy (and thus a small discretization length-scale) will be requested of any future nanocomposite model. For these reasons, this effort focuses on developing a reduced-order dynamic nanotube *finite element* suitable for incorporation into a general finite element framework.

Several computational models exist in the literature for simulating the mechanical response of a carbon nanotube which can be considered as candidate finite elements. Attention here will be focused narrowly on the literature detailing *computational* nanotube modeling. Comprehensive literature reviews which detail the current state-of-the-art of all other carbon nanotube and nanocomposite modeling approaches are provided by [Qian *et al.*, 2002] and [Srivastava *et al.*, 2003].

In addition to approaches using classical molecular dynamics [Iijima *et al.*, 1996; Yakobson *et al.*, 1997] or tight-binding molecular mechanics [Hernandez *et al.*, 1998], both of which result in elements which are prohibitively large in degrees of freedom, a number of reduced-order continuum-like computational approaches have also been developed. These approaches can be broadly separated into general (continuum) approaches and more-specific elasticity approaches in which the nanotube is modeled using elastic truss, beam, or shell theories. Numerous among the general approaches are those that bridge molecular mechanics and continuum mechanics, such as the quasi-continuum method [Tadmor *et al.*, 1996, 1999], the coarse-grained molecular dynamics method [Rudd and Broughton, 1998], the hand-shaking methods [Abraham *et al.*, 1998], [Belytschko and Xiao, 2003], the atomistic-continuum homogenization method [Chung and Namburu, 2003], and the Atomic-Scale Finite Element method [Liu *et al.*, 2004]. A structural mechanics approach [Li and Chou, 2003] has also been introduced which treats the nanotube's carbon-to-carbon bonds as sources of axial, bending, and torsional stiffness. Although these methods address directly, or can be

applied to, carbon nanotubes, they have not benefited significantly from dimension or order reduction and as a result, as pertains to this effort, contain a prohibitively large number of degrees of freedom.

Elasticity models have benefited from dimension and order reduction and can be further divided into one-dimensional truss-like/beam-like models and two-dimensional shell-like models. Truss and beam models similar to that detailed in [Odegard *et al*., 2002] have been used to determine a nanotube's effective axial, bending, and torsional rigidities. Extensions of these models have not been developed for obtaining a nanotube's response to general three-dimensional loading, as is desired here. However, shell models (in discretized form [Arroyo and Belytschko, 2002, 2003; Pantano *et al.*, 2004]) have been developed which are capable of simulating the three-dimensional equilibrium response of a carbon nanotube, to include buckling of the tube's inner wall in response to axial, bending, and torsional loading. It should be noted that to simulate inner wall buckling requires a large number of elements and a nanotube undergoing relatively large displacements. Considering that the average length of a nanotube is measurable in nanometers, the extreme degree of nanocomposite bulk deformation required to induce wall buckling should not be expected in nearly all applications. It is therefore reasonable to expect further gains in computational efficiency can be achieved, with little loss in accuracy, by reducing the dimension of the nanotube model and (importantly) considering a fully three-dimensional deformation state. The latter requires a state description capable of decomposing two components of curvature and one component of torsion, of which there are several.

The remainder of this work is concerned with developing such a model based on a recently developed *intrinsic* beam formulation [Hodges, 2003] together with a finite element discretization incorporating atomistic potentials. In addition to curvature and torsion, the model developed captures axial extension and simple two-axis cross-sectional shear. The developed model is also the first reduced-order CNT model known to the author capable of determining both static and dynamic responses to external loading.

2. CNT INTRINSIC FORMULATION

A finite element model for a carbon nanotube is developed next using an atomistic-based *intrinsic* formulation which follows closely the kinematics and governing equations of a recently developed anisotropic beam model [Hodges, 2003]. In the current context, intrinsic refers to a description of the nanotube configuration without reference to displacements and rotations, and instead with reference to curvatures and strains. This approach offers several advantages: 1) the resulting partial differential equations governing motion are in first-order form (i.e. have first-order time derivatives only), 2) the system nonlinearities appear at low order, 3) the intrinsic description incorporating curvature allows low-order interpolation functions to describe generally curved and twisted nanotube centerlines, unlike with a choice of an extrinsic description tied to displacements for which higher-order (and thus more degrees of freedom) interpolants are necessary, 4) inter-element displacements, slopes, and curvatures are matched at the element boundaries, and 5) finite rotational variables are absent, along with their inherit complexities. In addition, the developed model and a subsequent finite element discretization are able to capture the nanotube's dynamic response, without the expense of calculating the dynamic response of individual atoms as in Molecular Dynamics simulations.

Consider the initially curved and twisted nanotube, shown in Fig. 1, in which position along the centerline of the nanotube is given by $\boldsymbol{r}$ and for which a set of orthogonal unit basis vectors $\boldsymbol{b}_i$ are used to locate points away from the centerline. Tangent to the center-line is the basis vector $\boldsymbol{b}_1$ while $\boldsymbol{b}_2$, $\boldsymbol{b}_3$ are considered to be fixed in the nanotube cross-section. As such, distance along the centerline is denoted by x_1 and off-centerline points have at least one non-zero x_2, x_3. Spatial changes in this initial triad are given by $\boldsymbol{b}_i' = \boldsymbol{k} \times \boldsymbol{b}_i$ where $\boldsymbol{k}$ is the curvature vector with components k_i relative to $\boldsymbol{b}_i$ such that k_1 measures the initial twist and k_2, k_3 measure the $\boldsymbol{b}_2$, $\boldsymbol{b}_3$ components of the initial centerline curvature. In the deformed configuration, a new centerline $\boldsymbol{R}$ is measured by arc distance s while points on the deformed cross-section are referenced to the orthogonal unit basis vectors $\boldsymbol{B}_i$ where, due to cross-sectional shear, $\boldsymbol{B}_1$ is not tangential to $\boldsymbol{R}$. Instead, $\boldsymbol{B}_2$ and $\boldsymbol{B}_3$ are considered to be unit vectors in the direction of convected $\boldsymbol{b}_2$ and $\boldsymbol{b}_3$ and $\boldsymbol{B}_1$ is defined by $\boldsymbol{B}_1 = \boldsymbol{B}_2 \times \boldsymbol{B}_3$. Note that for small deformations, the x_1-spatial changes in the $\boldsymbol{B}_i$ basis can be expressed as $\boldsymbol{B}_i' = \boldsymbol{K} \times \boldsymbol{B}_i$ where $\boldsymbol{K}$ denotes the deformed configuration's curvature vector with components K_i relative to $\boldsymbol{B}_i$. In addition to the new centerline curvature, the centerline is allowed to stretch (as measured by strain component γ_{11}) and the nanotube cross-section is allowed to shear in both transverse directions (as measured by γ_{12} and γ_{13}. Together, the strain components are stored in a strain vector given by $\boldsymbol{\gamma} = [\gamma_{11}, \gamma_{12}, \gamma_{13}]^T$.

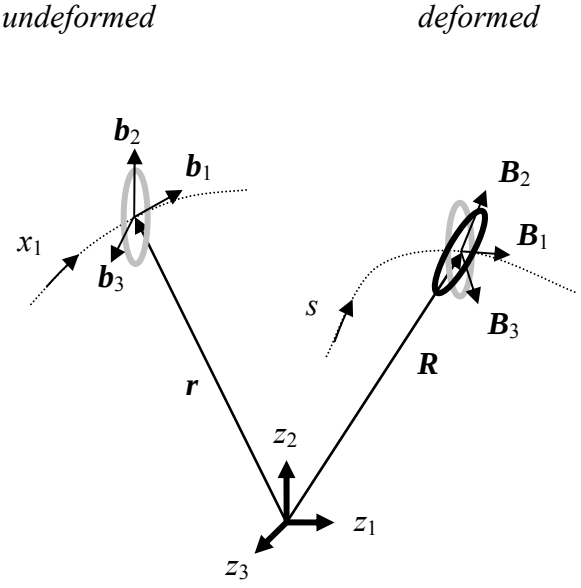

Figure 1: Geometry of a nanotube in the undeformed and deformed configurations.

The intrinsic equations of motion governing the nanotube response to external loads follow those presented by Hodges [2003] for an initially curved and twisted anisotropic beam,

$$\boldsymbol{F}' + \boldsymbol{K} \times \boldsymbol{F} + \boldsymbol{f} = \dot{\boldsymbol{P}} + \boldsymbol{\Omega} \times \boldsymbol{P}, \qquad (1a)$$

$$\boldsymbol{M}' + \boldsymbol{K}\times\boldsymbol{M} + (\boldsymbol{e_1}+\boldsymbol{\gamma})\times\boldsymbol{F} + \boldsymbol{m} = \dot{\boldsymbol{H}} + \boldsymbol{\Omega}\times\boldsymbol{H} + \boldsymbol{V}\times\boldsymbol{P} \quad (1b)$$

where all quantities are assumed to have x_1-dependence only such that this first set of equations relates x_1-spatial changes in the internal force resultant $\boldsymbol{F}$ and internal moment resultant $\boldsymbol{M}$, both acting on the deformed nanotube's cross-section, to the time rate-of-change of linear momentum per unit length $\boldsymbol{P}$ (associated with velocity $\boldsymbol{V}$) and angular momentum per unit length $\boldsymbol{H}$ (associated with angular velocity $\boldsymbol{\Omega}$). The net distributed forces per unit length are captured by $\boldsymbol{f}$, while the net distributed moments per unit length are captured by $\boldsymbol{m}$. Measured relative to $\boldsymbol{B}_i$ the unit vector $\boldsymbol{e_1}$ is given by $[1\ 0\ 0]^T$. A second set of equations relates x_1-spatial changes in the velocity $\boldsymbol{V}$ and angular velocity $\boldsymbol{\Omega}$ to time derivatives of the *net* curvature $\boldsymbol{\kappa}$ (i.e. $\boldsymbol{K}$ - $\boldsymbol{k}$) and the strain $\boldsymbol{\gamma}$,

$$\boldsymbol{\Omega}' + \boldsymbol{K}\times\boldsymbol{\Omega} = \dot{\boldsymbol{\kappa}}, \quad (1c)$$

$$\boldsymbol{V}' + \boldsymbol{K}\times\boldsymbol{V} + (\boldsymbol{e_1}+\boldsymbol{\gamma})\times\boldsymbol{\Omega} = \dot{\boldsymbol{\gamma}}. \quad (1d)$$

The general momenta and velocities are related through the mass per-unit-length μ, cross-sectional mass moments and product of inertia i_2, i_3, i_{23}; and centroidal offsets from the centerline $\bar{x}_2, \bar{x}_3$,

$$\begin{Bmatrix} P_1 \\ P_2 \\ P_3 \\ H_1 \\ H_2 \\ H_3 \end{Bmatrix} = \begin{bmatrix} \mu & 0 & 0 & 0 & \mu\bar{x}_3 & -\mu\bar{x}_2 \\ 0 & \mu & 0 & -\mu\bar{x}_3 & 0 & 0 \\ 0 & 0 & \mu & \mu\bar{x}_2 & 0 & 0 \\ 0 & -\mu\bar{x}_3 & \mu\bar{x}_2 & i_2+i_3 & 0 & 0 \\ \mu\bar{x}_3 & 0 & 0 & 0 & i_2 & i_{23} \\ -\mu\bar{x}_2 & 0 & 0 & 0 & i_{23} & i_3 \end{bmatrix} \begin{Bmatrix} V_1 \\ V_2 \\ V_3 \\ \Omega_1 \\ \Omega_2 \\ \Omega_3 \end{Bmatrix}, \quad (2)$$

where subscripts refer to the $\boldsymbol{B}_i$ basis vectors. Note that if position $\boldsymbol{X}$ of the nanotube centerline at any location x_1 is desired, $\boldsymbol{V}$ can be integrated with respect to time.

The formulation is completed with specification of (generally anisotropic) constitutive equations relating deformation metrics ($\boldsymbol{\kappa}$, $\boldsymbol{\gamma}$) to internal stress resultants ($\boldsymbol{F}$, $\boldsymbol{M}$). Herein, the constitutive relationship is derived directly from the nanotube crystalline structure and the atomistic potential energy function. Specifically, a strain energy function u per unit length is assumed such that

$$\boldsymbol{F} = \frac{\partial u}{\partial \boldsymbol{\gamma}}, \qquad \boldsymbol{M} = \frac{\partial u}{\partial \boldsymbol{\kappa}}. \quad (3)$$

As discussed in the next section, the bridge to atomistic mechanics is accomplished by equating strain energy density u to the energy of a four-atom representative volume element (rve) calculated using any appropriate atomistic potential.

3. ATOMISTIC-BASED CONSTITUTIVE MODELING

A carbon nanotube can be described as a graphene sheet rolled about a particular direction **C** described by the so-called *chiral* angle ϕ, as shown in Fig. 2. Graphene is a particular crystalline lattice form of carbon in which each carbon atom is bonded to three neighboring carbon atoms, forming a hexagonal arrangement. In Fig. 2, straight line segments depict the hybridized sp^2 bonds between the carbon atoms, while the carbon atoms themselves (not shown) exist at the intersections of the line segments. Accordingly, each hexagon holds six carbon atoms.

In general, a crystalline lattice L in its reference (unloaded) configuration is comprised of a number of interpenetrating Bravais lattices whose points are given by

$$\mathbf{X} = M^i\mathbf{a}_i + \mathbf{p}_k, \text{ with } i = 1, 2, 3, M^i \in Z, \quad (4)$$

where $\mathbf{X}$ are the lattice intersection points, $\mathbf{a}_i$ are the linearly independent (although not necessarily orthogonal) lattice vectors or Bravais base vectors, and $\mathbf{p}_k$ are the shift vectors for the inner atoms. For N+1 atoms in the basis, the index k runs from 0 to N [Zanzotto, 1992]. For graphene, two Bravais lattices are present and therefore k equals one. Note that since graphene is a planar crystal, only the base vectors $\mathbf{a}_1$ and $\mathbf{a}_2$ need be considered, where each has an undeformed length l_0 equal to $2.46\,\mathring{\mathrm{A}}$. These base vectors can be used to define the chiral vector **C**: (n,m). The length of the chiral vector is given by $C = \|\mathbf{C}\| = l_0\sqrt{n^2+nm+m^2}$, which when divided by 2π yields the nanotube radius r. Due to periodicity of the lattice, each choice of **C** defines a *unit cell*, which is defined to be the smallest rectangle defined by **C**, and a translate of **C**, such that all four corners of the unit cell coincide with an atomic lattice point. The translation vector is given by **T** whose length is well documented, see for example [Harris, 1999], and is given by,

$$T = \|\mathbf{T}\| = l_0\sqrt{n'^2+n'm'+m'^2} = \begin{cases} \sqrt{3}C/d_H & n-m \neq 3zd_H \\ \sqrt{3}C/(3d_H) & n-m = 3zd_H \end{cases}, \quad (5)$$

where d_H denotes the highest common divisor of n and m and z denotes any integer. The height h and width w of the unit cell will be used interchangeably with T and C. Note that many stable carbon nanotube configurations are known to exist which result in a variety of admissible radii (r's) and chiralities (ϕ's). Two configurations in particular are the armchair tubes [30 degree chiral angle ϕ; **C**: (n,n)] and the zig-zag tubes [zero degree chiral angle ϕ; **C**: (n,0)].

The stored potential energy of an atomistic system can be modeled using an appropriate atomistic potential function. These potentials typically see application in Molecular Dynamics (MD) simulations, but have also recently been applied to reduced-order or continuum-like models [Belytschko, *et al*., 2002; Zhang *et al*., 2002; Arroyo and Belytschko, 2003]. For a given set of interacting atoms, the atomistic potential function computes the atomistic energy based on bond lengths (i.e. two-body potentials), and in many cases, bond lengths and bond angles (i.e. three-body potentials). An alternative means to compute atomic energy is through use of the so-called Tight-binding models, which are simplified quantum-mechanical models. Tight-binding models are not incorporated into the present formulation.

Examples of commonly used potentials for carbon systems include the Morse potential, a two-body potential, and the Modified Morse and Brenner potentials [Brenner, 1990], three-body potentials. Although commonly accepted for carbon nanotubes, the Brenner potential does not exhibit a clear separation between the bond-generated energy and the angle-generated energy, which is necessary for calculating the energy of this work's representative volume element. A recent Modified Morse potential [Belytchsko *et al*., 2002] does have this feature, and is therefore the potential chosen for this work. The potential is detailed in Section 3.2.

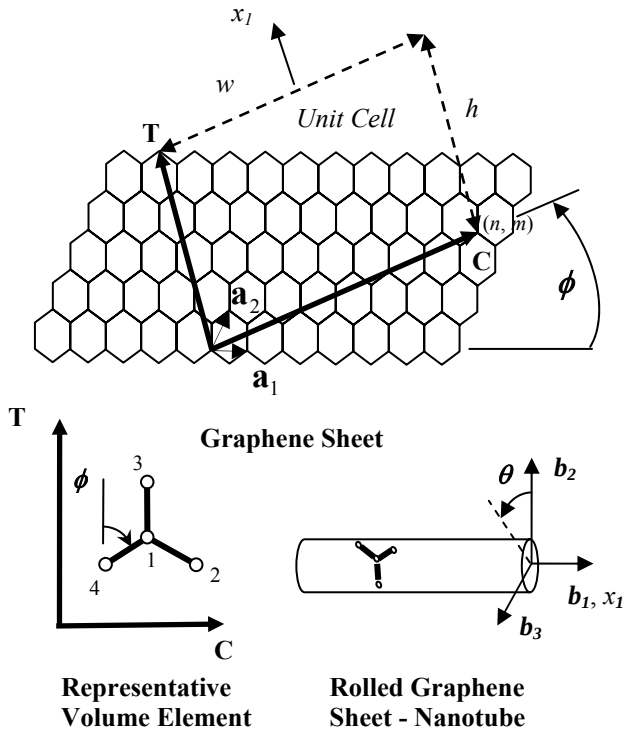

Figure 2: Geometry of the graphene sheet; representative volume element; tube.

3.1 Configuration Kinematics

In order to implement the chosen atomistic potential function, the relative position of any two atoms away from the deformed centerline must be known. These relative positions can then be used to identify the bond length and, using three atoms, the bond angles. Ideally, in keeping with the intrinsic nature of the formulation, these relative positions should be expressed in terms of the intrinsic metrics net curvature $\boldsymbol{\kappa}$ and strain $\boldsymbol{\gamma}$. This is accomplished by introducing an expansion of the atomic position vectors and the basis vectors $\boldsymbol{B}_i(x_1)$, as follows. For brevity, presentation of the expansion is limited to low orders. However, in order to capture the center-line's dependence on geometric torsion[1], the numerically implemented expansions are up to and including $O(dx_1^3)$ terms.

To start, consider the position vector in the deformed configuration $\boldsymbol{R}^*(x_1)$ of any point on the cross-section originally occupying material point (x_1, $x_2(x_1)=a_2$, $x_3(x_1)= a_3$) and the position vector $\boldsymbol{R}^*(x_1+dx_1)$ of any second point originally occupying material point ($x_1 + dx_1$, $x_2(x_1 + dx_1)=b_2$, $x_3(x_1 + dx_1) =b_3$). It is convenient to express $\boldsymbol{R}^*(x_1)$ using the centerline position $\boldsymbol{R}(x_1)$ such that in the deformed configuration,

$$\boldsymbol{R}^*(x_1;a_2,a_3)=\boldsymbol{R}(x_1)+\big(2\gamma_{12}(x_1)a_2+2\gamma_{13}(x_1)a_3\big)\boldsymbol{B_1}(x_1) + a_2\boldsymbol{B_2}(x_1)+a_3\boldsymbol{B_3}(x_1), \quad (6)$$

where it is noted that additional cross-sectional warping with x_2-, x_3-dependence [Hodges, 1990] is considered a secondary effect and is therefore not included in the kinematical description of the nanotube deformation. In a similar manner, $\boldsymbol{R}^*(x_1+dx_1)$ can be expressed as,

$$\boldsymbol{R}^*(x_1+dx_1;b_2,b_3)=\boldsymbol{R}(x_1+dx_1)+b_2\boldsymbol{B_2}(x_1+dx_1)+b_3\boldsymbol{B_3}(x_1+dx_1) + \big(2\gamma_{12}(x_1+dx_1)b_2+2\gamma_{13}(x_1+dx_1)b_3\big)\boldsymbol{B_1}(x_1+dx_1). \quad (7)$$

In order to calculate distances and angles using $\boldsymbol{R}^*(x_1)$ and $\boldsymbol{R}^*(x_1+dx_1)$, $\boldsymbol{R}^*(x_1+dx_1)$ must be expressed in terms of the basis vectors $\boldsymbol{B}_i$ at x_1. This can be accomplished using a Taylor expansion applied to both $\boldsymbol{B_i}(x_1+dx_1)$ and to $\boldsymbol{R}(x_1+dx_1)$. Note that it is critical to expand both the position vector and the basis vectors, as opposed to just the position vector as per deriving the local canonical form of a space curve. As an illustration, consider a bending deformation for which the change in length of an arc segment away from the centerline would not be accounted for if $\boldsymbol{B_2}(x_1+dx_1)$, $\boldsymbol{B_3}(x_1+dx_1)$ remained oriented with $\boldsymbol{B_2}(x_1)$, $\boldsymbol{B_3}(x_1)$. The basis vectors can be expanded to $O(dx_1^3)$ as,

$$\boldsymbol{B_i}(x_1+dx_1)=\boldsymbol{B_i}(x_1)+\boldsymbol{B_i'}(x_1)dx_1+\frac{1}{2}\boldsymbol{B_i''}(x_1)dx_1^2+O(dx_1^3)=$$

$$\boldsymbol{B_i}(x_1)+\big(\boldsymbol{K}(x_1)\times\boldsymbol{B_i}(x_1)\big)dx_1 + \frac{1}{2}\big(\boldsymbol{K}(x_1)\times\big(\boldsymbol{K}(x_1)\times\boldsymbol{B_i}(x_1)\big)+\boldsymbol{K'}(x_1)\times\boldsymbol{B_i}(x_1)\big)dx_1+O(dx_1^3), \quad (8)$$

and the centerline position can be expanded as

$$\boldsymbol{R}(x_1+dx_1)=\boldsymbol{R}(x_1)+\boldsymbol{R'}(x_1)dx_1+\frac{1}{2}\boldsymbol{R''}(x_1)dx_1^2+O(dx_1^3)=\boldsymbol{R}(x_1)+$$

$$\boldsymbol{B_1}(x_1)dx_1+\frac{1}{2}K_3(x_1)\boldsymbol{B_2}(x_1)dx_1^2-\frac{1}{2}K_2(x_1)\boldsymbol{B_3}(x_1)dx_1^2+O(dx_1^3), \quad (9)$$

where for small strains $\boldsymbol{R'}(x_1)=\boldsymbol{B_1}$ and $\boldsymbol{R''}(x_1)=\boldsymbol{B_1'}=\boldsymbol{K}\times\boldsymbol{B_1}=K_3\boldsymbol{B_2}-K_2\boldsymbol{B_3}$ has been used. Using both expansions together with expansions for $\gamma_{12}(x_1+dx_1)$ and $\gamma_{13}(x_1+dx_1)$, the final expression for $\boldsymbol{R}^*(x_1+dx_1)$ is given as,

$$\begin{aligned}\boldsymbol{R}^*(x_1+dx_1;b_2,b_3)&=\boldsymbol{R}(x_1)\\&+\big[2\big(\gamma_{12}+\gamma_{12}'dx_1\big)b_2+2\big(\gamma_{13}+\gamma_{13}'dx_1\big)b_3+\big(1-b_2K_3+b_3K_2\big)dx_1\big]\boldsymbol{B_1}(s)\\&+\big[b_2+\big(-b_3K_1+2\gamma_{12}b_2K_3+2\gamma_{13}b_3K_3\big)dx_1\big]\boldsymbol{B_2}(x_1)\\&+\big[b_3+\big(b_2K_1-2\gamma_{12}b_2K_2-2\gamma_{13}b_3K_2\big)dx_1\big]\boldsymbol{B_3}(x_1)+O(dx_1^2)\end{aligned} \quad (10)$$

From (6) and (10), the relative position $\boldsymbol{r_{ab}}$ of two atomic positions in the deformed configuration can now be given by,

$$\begin{aligned}\boldsymbol{r_{ab}}&=\big[2\gamma_{12}(b_2-a_2)+2\gamma_{13}(b_3-a_3)+\big(1+2\gamma_{12}'b_2+2\gamma_{13}'b_3-b_2K_3+b_3K_2\big)dx_1\big]\boldsymbol{B_1}(x_1)\\&+\big[(b_2-a_2)+\big(-b_3K_1+2\gamma_{12}b_2K_3+2\gamma_{13}b_3K_3\big)dx_1\big]\boldsymbol{B_2}(x_1)\\&+\big[(b_3-a_3)+\big(b_2K_1-2\gamma_{12}b_2K_2-2\gamma_{13}b_3K_2\big)dx_1\big]\boldsymbol{B_3}(x_1)+O(dx_1^2).\end{aligned} \quad (11)$$

With development of an intrinsic relative position measure $\boldsymbol{r_{ab}}$, the bond lengths and bond angles are expressed in terms of the intrinsic deformation metrics,

$$r_{ab}=\|\boldsymbol{r_{ab}}\|, \quad \cos(\theta_{abc})=\frac{\boldsymbol{r_{ab}}\cdot\boldsymbol{r_{ac}}}{\|\boldsymbol{r_{ab}}\|\,\|\boldsymbol{r_{ac}}\|}. \quad (12)$$

3.2 Modified Morse Potential

The atomistic potential chosen for this study is a Modified Morse Potential [Belytchsko *et al*., 2002], although it is noted

[1] Inspection of the local canonical form, e.g. [do Carmo, 1976], reveals that geometric torsion first appears at $O(ds^3)$.

that the formulation is not dependent on any specific atomistic potential. As discussed in [Belytchsko *et al*., 2002], if the classical Morse Potential is to be used for modeling CNT's, a three-body term accounting for angular position must be included in order to stabilize a tubular position. As such, the modified potential then takes the form,

$$E = E_{stretch} + E_{angle}\ ;\ \ E_{stretch} = D_e\left\{\left[1-e^{-\beta(r-r_0)}\right]^2 - 1\right\};$$
$$E_{angle} = \frac{1}{2}k_\theta(\theta-\theta_0)^2\left[1+k_{sextic}(\theta-\theta_0)^4\right] \qquad (13)$$

where $E_{stretch}$ is the bond energy due to bond stretch, E_{angle} is the bond energy due to bond angle-bending, r is the length of the bond, and θ is the current angle of the adjacent bond. The parameters used in all simulations herein correspond to sp^2 bonds and are given by

$$r_0 = 1.39\times10^{-10}\,\text{m};\quad D_e = 6.03105\times10^{-19}\,\text{Nm};$$
$$\beta = 2.625\times10^{10}\,\text{m}^{-1};\quad \theta_0 = 2.094\,\text{rad};$$
$$k_\theta = 0.9\times10^{-18}\,\text{Nm/rad}^2;\quad k_{sextic} = 0.754\ \text{rad}^{-4}.$$

Performance of this potential for strains below 10% has been shown to compare very well [Belytchsko *et al*., 2002] to the more commonly accepted Brenner potential [Brenner, 1990] – the advantage of adopting the Modified Morse Potential is that the stretching and angular contributions are distinct, which is important when forming a representative volume element, as discussed next.

3.3 Representative Volume Element

The connection between the deformation state variables $(\boldsymbol{V}, \boldsymbol{\Omega}, \boldsymbol{\kappa}, \boldsymbol{\gamma})$ and the stored atomic energy can be made using representative volume elements at locations x_1. In turn, strain energy density per unit length u is connected to rve atomistic energy E^{rve} as follows,

$$u = \frac{E^{rve}}{l^{rve}}, \qquad (14)$$

where l^{rve} is a characteristic length of the rve. Note that for each x_1 in which the internal forces $\boldsymbol{F}$ and moments $\boldsymbol{M}$ are to be calculated, several rve's should be evaluated (and energy averaged) corresponding to several locations on the nanotube surface. In this way, using bending as an example, stretching of atomic bonds at one location on the perimeter, and compression of atomic bonds at an opposing location, is appropriately captured.

Following the development of [Arroyo and Belytchsko, 2003], a four-atom rve is chosen as shown in Fig. 2. In contrast to [Arroyo and Belytchsko, 2003], the present approach requires a strain energy density *per unit length*, which is developed as follows. The chosen rve consists of three bond lengths and three bond angles covering completely the three bond length and angle varieties in each graphene hexagon. However, for the graphene hexagons, every bond length is shared by two hexagons, while each bond angle is unique to each hexagon. As such, the three rve bonds represent the three *net* bond lengths contained in a single graphene hexagon, while the three rve angles represent only half of the *net* bond angles in the same graphene hexagon. This dictates that an energy per unit area be defined as,

$$e^{rve} \equiv \frac{E^{rve}}{A_{Hex}} = \frac{E^{rve}_{stretch} + 2E^{rve}_{angle}}{A_{Hex}}, \qquad (15)$$

where $E^{rve}_{stretch}$ is calculated from the Modified Morse Potential summing the stretch energy from the three rve bond lengths, E^{rve}_{angle} is calculated summing the angle-bending energy using the three rve bond angles, and A_{Hex} represents the area of the graphene hexagon (5.019743 Å^2). The final desired expression for energy per unit length u can now be formed from the unit cell dimensions width w and height h,

$$u = \frac{e^{rve}\cdot h\cdot w}{h} = e^{rve}\cdot w = \frac{E^{rve}_{stretch} + 2E^{rve}_{angle}}{A_{Hex}}\cdot w. \qquad (16)$$

For completeness of the discussion, the rve characteristic length is identified from (14) and (16) as $l^{rve} = A_{Hex}/w$.

To calculate the internal forces and moments, derivatives of u with respect to the deformations $\boldsymbol{\gamma}$ and $\boldsymbol{\kappa}$ must be formed. These derivatives can be calculated as follows,

$$\boldsymbol{F} = \frac{\partial u}{\partial \boldsymbol{\gamma}} = \frac{w}{A_{Hex}}\left(\frac{\partial E^{rve}_{stretch}}{\partial r_{ij}}\frac{\partial r_{ij}}{\partial \boldsymbol{\gamma}} + 2\frac{\partial E^{rve}_{angle}}{\partial \theta_{ijk}}\frac{\partial \theta_{ijk}}{\partial \boldsymbol{\gamma}}\right),$$
$$\boldsymbol{M} = \frac{\partial u}{\partial \boldsymbol{\kappa}} = \frac{w}{A_{Hex}}\left(\frac{\partial E^{rve}_{stretch}}{\partial r_{ij}}\frac{\partial r_{ij}}{\partial \boldsymbol{\kappa}} + 2\frac{\partial E^{rve}_{angle}}{\partial \theta_{ijk}}\frac{\partial \theta_{ijk}}{\partial \boldsymbol{\kappa}}\right), \qquad (17)$$

where i,j,k are indices representing the four rve atoms such that the non-zero bond lengths r_{ij} include only $\{r_{12}, r_{13}, r_{14}\}$ and the non-zero bond angles θ_{ijk} include only $\{\theta_{123},\ \theta_{124},\ \theta_{134}\}$. These quantities can be calculated from the deformation state using the procedure described in Section 3.1, while the complexity associated with finding closed-form expressions for their derivatives with respect to $\boldsymbol{\gamma}$ and $\boldsymbol{\kappa}$ will require finite difference approximations in the numerical implementation.

With the viewpoint that atom 1 is located at x_1, and that the other three atoms are located a small distance dx_1 away, the parameters $\{x_1,\ dx_1,\ a_2,\ a_3,\ b_2,\ b_3\}$ required to evaluate the expressions in Section 3.1 are as follows:

$$x_1^{(1)} = {}^0x_1^{(1)} + \eta_{x_1},\ \theta^{(1)} = {}^0\theta^{(1)} + \eta_\theta,\ a_2^{(1)} = r\cos(\theta^{(1)}),$$
$$a_3^{(1)} = r\cos(\theta^{(1)}), \qquad (18a)$$

$$dx_1^{(2)} = {}^0b\cos\left(\frac{\pi}{3}+\phi\right) + \eta_{x_1}\ \theta^{(2)} = {}^0\theta^{(1)} + \frac{{}^0b}{r}\sin\left(\frac{\pi}{3}+\phi\right),$$
$$b_2^{(2)} = r\cos(\theta^{(2)}),\ \ b_3^{(2)} = r\cos(\theta^{(2)}), \qquad (18b)$$

$$dx_1^{(3)} = {}^0b\cos\left(\phi-\frac{\pi}{3}\right) + \eta_{x_1}\ \theta^{(3)} = {}^0\theta^{(1)} + \frac{{}^0b}{r}\sin\left(\phi-\frac{\pi}{3}\right),$$
$$b_2^{(3)} = r\cos(\theta^{(3)}),\ \ b_3^{(3)} = r\cos(\theta^{(3)}), \qquad (18c)$$

$$dx_1^{(4)} = -{}^0b\cos(\phi) + \eta_{x_1}\ \theta^{(4)} = {}^0\theta^{(1)} - \frac{{}^0b}{r}\sin(\phi),\ b_2^{(4)} = r\cos(\theta^{(4)}),$$
$$b_3^{(4)} = r\cos(\theta^{(4)}), \qquad (18d)$$

where the atom referenced is indicated by a right superscript in parentheses, an initial location at the start of the simulation is referenced by a left superscript zero, θ refers to an angular measure counter clock-wise away from the x_2-axis, the initial bond length is denoted by ${}^0b$ (1.39 Å), and inner

displacements (discussed in the next section) of atom 1 in the x_1 and θ directions are denoted by η_{x_1} and η_θ, respectively.

3.4 Inner Displacements

For large deformations, the Bravais multi-lattice should be relaxed using inner displacements [Tadmor; Arroyo and Belytchsko, 2003]. These inner displacements allow atom 1 to move relative to atoms 2, 3, and 4 such that a lower minimum energy state can be achieved – this is equivalent to one of the lattices moving rigidly relative to the other. Use of the inner displacements in the formulation is discussed in Section 5.2, while results in which the rve is relaxed, versus left unrelaxed, are presented in Section 6.

4. FINITE ELEMENT FORMULATION

The first-order governing equations are now specialized to the case of a nanotube in an initially straight configuration (i.e. $\boldsymbol{\kappa} = \boldsymbol{K}$). Further simplification of the equations results when the mass of the atoms is locally averaged over the nanotube surface, in which case the mass center of any cross-section is located on the centerline (i.e. $\bar{x}_2 = \bar{x}_3 = 0$), and the cross-section has radial symmetry (i.e. $i_{23} = 0$). Note that this simplification becomes increasingly more appropriate as the nanotube radius increases, and thereby the number of atoms increases. With the above simplifications the governing equations reduce to,

$$\mu\dot{\boldsymbol{V}} = \boldsymbol{F}' + \boldsymbol{K}\times\boldsymbol{F} + \boldsymbol{f} - \boldsymbol{\Omega}\times\mu\boldsymbol{V}\,, \tag{19a}$$

$$\begin{bmatrix} i_1\dot{\Omega}_1 \\ i_2\dot{\Omega}_2 \\ i_3\dot{\Omega}_3 \end{bmatrix} = \boldsymbol{M}' + \boldsymbol{K}\times\boldsymbol{M} + (\boldsymbol{e_1}+\boldsymbol{\gamma})\times\boldsymbol{F} + \boldsymbol{m} - \boldsymbol{\Omega}\times\begin{bmatrix} i_1\Omega_1 \\ i_2\Omega_2 \\ i_3\Omega_3 \end{bmatrix}, \tag{19b}$$

$$\dot{\boldsymbol{K}} = \boldsymbol{\Omega}' + \boldsymbol{K}\times\boldsymbol{\Omega}\,, \tag{19c}$$

$$\dot{\boldsymbol{\gamma}} = \boldsymbol{V}' + \boldsymbol{K}\times\boldsymbol{V} + (\boldsymbol{e_1}+\boldsymbol{\gamma})\times\boldsymbol{\Omega}\,, \tag{19d}$$

where $i_1 \equiv i_2 + i_3$ has been introduced.

The governing equations as stated above, with an appropriate selection of boundary conditions, denote a so-called *strong form*. The *weak form* is more convenient from a finite element standpoint and can be developed from the strong form using *virtual* velocities and deformation measures $\delta\boldsymbol{V}$ and $\delta\boldsymbol{\Omega}$. Unlike the actual velocities, the virtual velocities are allowed to satisfy homogenous boundary conditions at the domain ends. Taking the inner product of each equation with the appropriate virtual quantity yields the following weak form,

$$\int \mu\dot{\boldsymbol{V}}\cdot\delta\boldsymbol{V}\; dx_1 = \int \left(\boldsymbol{F}' + \boldsymbol{K}\times\boldsymbol{F} + \boldsymbol{f} - \boldsymbol{\Omega}\times\mu\boldsymbol{V}\right)\cdot\delta\boldsymbol{V}\; dx_1\,, \tag{20a}$$

$$\int \begin{bmatrix} i_1\dot{\Omega}_1 \\ i_2\dot{\Omega}_2 \\ i_3\dot{\Omega}_3 \end{bmatrix}^T \begin{bmatrix} \delta\Omega_1 \\ \delta\Omega_2 \\ \delta\Omega_3 \end{bmatrix} dx_1 =$$

$$\int \left(\boldsymbol{M}' + \boldsymbol{K}\times\boldsymbol{M} + (\boldsymbol{e_1}+\boldsymbol{\gamma})\times\boldsymbol{F} + \boldsymbol{m} - \boldsymbol{\Omega}\times\begin{bmatrix} i_1\Omega_1 \\ i_2\Omega_2 \\ i_3\Omega_3 \end{bmatrix} \right)^T \begin{bmatrix} \delta\Omega_1 \\ \delta\Omega_2 \\ \delta\Omega_3 \end{bmatrix} dx_1\,, \tag{20b}$$

$$\int \dot{\boldsymbol{K}}\cdot\delta\boldsymbol{\Omega}\; dx_1 = \int \left(\boldsymbol{\Omega}' + \boldsymbol{K}\times\boldsymbol{\Omega}\right)\cdot\delta\boldsymbol{\Omega}\; dx_1\,, \tag{20c}$$

$$\int \dot{\boldsymbol{\gamma}}\cdot\delta\boldsymbol{V}\; dx_1 = \int \left(\boldsymbol{V}' + \boldsymbol{K}\times\boldsymbol{V} + (\boldsymbol{e_1}+\boldsymbol{\gamma})\times\boldsymbol{\Omega}\right)\cdot\delta\boldsymbol{V}\; dx_1\,. \tag{20d}$$

Spatial derivatives of the non-interpolated internal forces can be shifted to the virtual velocities through an integration by parts. Applying the homogenous boundary conditions to the virtual velocities allows the first two governing equations to be rewritten as,

$$\int \mu\dot{\boldsymbol{V}}\cdot\delta\boldsymbol{V}\; dx_1 = -\int \boldsymbol{F}'\cdot\delta\boldsymbol{V}'\, dx_1 + \int \left(\boldsymbol{K}\times\boldsymbol{F} + \boldsymbol{f} - \boldsymbol{\Omega}\times\mu\boldsymbol{V}\right)\cdot\delta\boldsymbol{V}\; dx_1\,, \tag{21a}$$

$$\int \begin{bmatrix} i_1\dot{\Omega}_1 \\ i_2\dot{\Omega}_2 \\ i_3\dot{\Omega}_3 \end{bmatrix}^T \begin{bmatrix} \delta\Omega_1 \\ \delta\Omega_2 \\ \delta\Omega_3 \end{bmatrix} dx_1 = -\int \boldsymbol{M}\cdot\begin{bmatrix} \delta\Omega_1' \\ \delta\Omega_2' \\ \delta\Omega_3' \end{bmatrix} dx_1 +$$

$$\int \left(\boldsymbol{K}\times\boldsymbol{M} + (\boldsymbol{e_1}+\boldsymbol{\gamma})\times\boldsymbol{F} + \boldsymbol{m} - \boldsymbol{\Omega}\times\begin{bmatrix} i_1\Omega_1 \\ i_2\Omega_2 \\ i_3\Omega_3 \end{bmatrix} \right)^T \begin{bmatrix} \delta\Omega_1 \\ \delta\Omega_2 \\ \delta\Omega_3 \end{bmatrix} dx_1\,. \tag{21b}$$

Next the center-line distance x_1, the deformation state measures ($\boldsymbol{V}, \boldsymbol{\Omega}, \boldsymbol{K}, \boldsymbol{\gamma}$) and the virtual velocities ($\delta\boldsymbol{V}, \delta\boldsymbol{\Omega}$) are interpolated for an element, $x_1 = [0, l]$, in the usual manner using shape functions $N_I(\xi)$ and nodal values,

$$x_1 = N_I(\xi)\, x_1^I,\ \boldsymbol{V} = N_I(\xi)\,\boldsymbol{V}^I,\ \boldsymbol{\Omega} = N_I(\xi)\,\boldsymbol{\Omega}^I,$$
$$\boldsymbol{K} = N_I(\xi)\,\boldsymbol{K}^I,\ \boldsymbol{\gamma} = N_I(\xi)\,\boldsymbol{\gamma}^I, \delta\boldsymbol{V} = N_J(\xi)\delta V^J,$$
$$\delta\boldsymbol{\Omega} = N_J(\xi)\delta\Omega^J\,, \tag{22}$$

where ξ represents a natural coordinate assuming values from -1 to 1 and where nodal quantities are indicated by a superscript I or J ranging from 1 to n, the number of element nodes. Repeated indices denote summation in the usual sense. Introducing the interpolated quantities into the governing equations, evaluating inner products, and recognizing that the expressions must hold for all allowable virtual velocity fields results in the semi-discrete equations,

$$\mu a^{JI}\dot{V}_k^I = \widetilde{F}_k^J - \mu c^{JIK}\Omega_i^I V_j^K e_{ijk}\,, \tag{23a}$$

$$a^{JI}\underbrace{i_k\dot{\Omega}_k^I}_{\substack{\text{no sum} \\ \text{on } k}} = \widetilde{M}_k^J - c^{JIK}\Omega_i^I\underbrace{(i_j\Omega_j^K)}_{\substack{\text{no sum} \\ \text{on } j}} e_{ijk}\,, \tag{23b}$$

$$a^{JI}\dot{K}_k^I = b^{JI}\Omega_k^I + c^{JIK}K_i^I\Omega_j^K e_{ijk}\,, \tag{23c}$$

$$a^{JI}\dot{\gamma}_k^I = b^{JI}V_k^I + c^{JIK}K_i^I V_j^K e_{ijk} + c^{JIK}\left(\gamma_i^I + \delta_{i1}\right)\Omega_j^K e_{ijk}\,, \tag{23d}$$

where

$$a^{JI} = \int_{-1}^{1} N_J N_I J d\xi\,,\ b^{JI} = \int_{-1}^{1} N_J N_{I,\xi}\frac{\partial\xi}{\partial x_1} J d\xi\,,$$
$$c^{JIK} = \int_{-1}^{1} N_J N_I N_K J d\xi\,,\ \text{with } J = \left|\frac{dx_1}{d\xi}\right| \tag{24}$$

are quantities which are invariant with respect to the deformation state (i.e. in the subsequent simulations can be calculated initially and re-used at each later time interval), e_{ijk} denotes the permutation index operator and δ_{i1} denotes the Kronecker delta, and internal force terms requiring integration are represented by the quantities $\widetilde{F}_k^J$ and $\widetilde{M}_k^J$ given explicitly by,

$$\widetilde{F}_k^J = \int_{-1}^{1}\left(-F_k N_J' + N_I N_J K_i^I F_j e_{ijk} + f_k N_J\right) J d\xi\,, \tag{25a}$$

$$\widetilde{M}_k^J = \int_{-1}^{1}(-M_k N_J' + N_I N_J K_i^I M_j e_{ijk}$$

$$+ N_I N_J \left(\gamma_i^I + \delta_{i1}\right) F_j e_{ijk} + m_k N_J) J d\xi \,. \qquad (25b)$$

In all expressions, the free indices J (not to be confused with the Jacobian $\mathcal{J}$ appearing in the integrals) and k indicate $3n$ nonlinear first-order equations. In the temporal integration of the semi-discrete equations, (25a,b) are integrated spatially using Gauss integration with the internal forces and moments being calculated via multiple representative volume elements at each Gauss point, as discussed in Section 5.1.

5. IMPLEMENTATION FOR A THREE-NODED ELEMENT

The formal finite element formulation detailed in Section 4 has been implemented in the form of a three-noded nanotube element integrated temporally using a 2nd order-accurate Heun Predictor-Corrector integration. Multiple elements are assembled using a standard procedure [Hughes, 1987]. Note that the assembly enforces continuity of the deformation state and hence the elements exhibit a high-degree of inter-element continuity - strains and curvatures are continuous across element boundaries. This is in contrast to only displacement, and possibly slope, continuity as seen in more traditional beam-like formulations.

5.1 Shape Functions and Constants

The shape functions used for the three-noded element are given as follows,

$$N_1 = \frac{1}{2}\xi(\xi - 1), \quad N_2 = 1 - \xi^2, \quad N_3 = \frac{1}{2}\xi(\xi + 1), \qquad (26)$$

where each shape function evaluates to one at its home location and zero at other nodal locations. Various quantities can now be evaluated. The expressions a^{JI}, b^{JI}, and c^{JIK} are functions of undeformed arc length x_1 and therefore need only be computed once and retained for the entire length of the simulation. If the Jacobian $\mathcal{J}$ is approximated as constant (this is exact for two-noded elements with linear shape functions), the tabulated numerical values for a^{JI}, b^{JI} given in Table 1 can be used for all three-node elements, with best performance expected in cases where nodes are evenly spaced. Twenty-seven values for c^{JIK} are also calculated, but are not presented here in the interest of brevity.

Calculation of $\widetilde{F}_k^J$ and $\widetilde{M}_k^J$ is dependent on the current deformation state of the element and must be performed at each time step. These expressions are computed using a Gauss quadrature routine where at each x_1 Gauss point the energy of four equally distributed (perimeter-wise) rve's is computed and averaged, as per the discussion of Section 3.3. Considerable efficiency gains can be achieved by calculating some of the derivatives present in (17) using finite differences, and saving the results for re-use over multiple time steps. Since small time steps will be taken using an explicit procedure, little error is introduced in doing so if the total elapsed time between recalculation (and thus the change in the deformation state) is small. This strategy is carried out for $\frac{\partial r_{ij}}{\partial \boldsymbol{\gamma}}$, $\frac{\partial \theta_{ijk}}{\partial \boldsymbol{\gamma}}$, $\frac{\partial r_{ij}}{\partial \boldsymbol{\kappa}}$, and $\frac{\partial \theta_{ijk}}{\partial \boldsymbol{\kappa}}$ at each of the four rve's at each Gauss point. Note that closed-from expressions are easily derived for $\frac{\partial E_{stretch}^{rve}}{\partial r_{ij}}$ and $\frac{\partial E_{angle}^{rve}}{\partial \theta_{ijk}}$ and therefore these expressions are evaluated exactly at each time step.

a^{JI}	**I = 1**	**I = 2**	**I = 1**
J = 1	$\frac{2}{15}l$	$\frac{1}{15}l$	$-\frac{1}{30}l$
J = 2	$\frac{1}{15}l$	$\frac{8}{15}l$	$\frac{1}{15}l$
J = 3	$-\frac{1}{30}l$	$\frac{1}{15}l$	$\frac{2}{15}l$

b^{JI}	**I = 1**	**I = 2**	**I = 1**
J = 1	$-\frac{1}{4}l$	$\frac{1}{3}l$	$-\frac{1}{12}l$
J = 2	$-\frac{1}{3}l$	0	$\frac{1}{3}l$
J = 3	$\frac{1}{12}l$	$-\frac{1}{3}l$	$\frac{1}{4}l$

Table 1: Tabulated coefficients for the three-noded element where l is the element length.

5.2 Inner Displacements

An inner displacement calculation can also be done at each time step that new values of $\frac{\partial r_{ij}}{\partial \boldsymbol{\gamma}}$, $\frac{\partial \theta_{ijk}}{\partial \boldsymbol{\gamma}}$, $\frac{\partial r_{ij}}{\partial \boldsymbol{\kappa}}$, and $\frac{\partial \theta_{ijk}}{\partial \boldsymbol{\kappa}}$ are calculated. The inner displacements of the Bravais lattices, η_{x_1} and η_θ, at each of the four rve's at each Gauss point, are found using a Newton-Raphson routine which computes the η_{x_1} and η_θ required to minimize the rve energy. During this calculation, the deformation state ($\boldsymbol{K}, \boldsymbol{\gamma}$) and the current time are held constant. Note that for small deformations, inner displacements may be unnecessary for the rve energy to be approximately stationary.

5.3 Temporal Integration

The semi-discrete finite element equations (23) must still be integrated temporally to compute the nanotube response. In this study, an explicit 2nd order-accurate Heun Predictor-Corrector algorithm, incorporating a lumped mass matrix, has

been chosen for the computations. Casting (23) into the standard form

$$[\mathbf{M}]\cdot\frac{d\mathbf{y}}{dt}=\mathbf{f}(\mathbf{y},t),$$

where $[\mathbf{M}]$ has been diagonalized using the "special lumping technique" [2] [Hughes, 1987], the integration in time proceeds with two steps. First, a predictor $\tilde{\mathbf{y}}_{n+1}$ is computed via,

$$\tilde{\mathbf{y}}_{n+1}=\mathbf{y}_n+[\mathbf{M}^{-1}]\cdot(\Delta t\cdot\mathbf{f}(\mathbf{y}_n,t_n)),$$

where subscript n denotes an already-calculated value at a previous time t_n, t_{n+1} denotes the current time, Δt denotes the time step, and $[\mathbf{M}^{-1}]$ is a trivial inverse in the sense that $[\mathrm{M}^{-1}]_{ii}=1/\mathrm{M}_{ii}$, no sum on i intended. The corrector step then follows to yield the desired state at t_{n+1},

$$\mathbf{y}_{n+1}=\mathbf{y}_n+\frac{\Delta t}{2}[\mathbf{M}^{-1}]\cdot(\mathbf{f}(\mathbf{y}_n,t_n)+\mathbf{f}(\tilde{\mathbf{y}}_{n+1},t_{n+1}))\cdot$$

6. Example Simulation Results

Although the formulated nanotube element is expected to be incorporated into a more general framework capable of evaluating the mechanical response of a nanocomposite (e.g. fiber-like nanotubes embedded in a traditional matrix material), example simulations of a (10,10) armchair in vacuum are presented in this section in order to assess the accuracy of the formulation, and to illustrate the nanotube's inherent response to a variety of loading. Simulations are presented for moderate deformation of the order likely in a typical composite material application. Specific focus is on the equilibrium configuration of the simulated nanotube, for which the results can be readily compared to similar results in the literature, and hence damping is introduced into the simulations. The damping is not necessary for numerical stability, and in fact, all damping is decreased until none exists in the later time increments. Undamped, or nearly undamped, vibration response of a carbon nanotube will be considered in a follow-up study. Here, damping is introduced through proportional damping elements which simply resist relative nodal changes in $V_k, \Omega_k, K_k, \gamma_k$ [3] while mass-scaling is utilized to increase the stable time step individually for each equation. Note that eight damping elements exist for each three-noded nanotube element – two rectilinear damping elements situated between local nodes one and two, and between local nodes two and three; similarly two rotational damping elements, two curvature damping elements, and two strain damping elements. For all simulations presented, four-point Gauss quadrature is employed when integrating to compute $\tilde{F}_k^J$ and $\tilde{M}_k^J$, and a three element (equal) discretization is used to represent the nanotube, although the development is general enough to include any number of Gauss points or elements. The parameter space for the (10,10) nanotube is given in Table 2 while a depiction of the nanotube discretization is shown in Fig. 3.

l (Å)	r (Å)	μ (amu/Å)	i_1 (amu Å)	i_2 (amu Å)	i_3 (amu Å)
300	6.875	710	7100	7100	7100

d_V ($\sqrt{\text{amu}\cdot\text{eV}}$/Å)	d_Ω (Å$\sqrt{\text{amu}\cdot\text{eV}}$)	d_K ($\sqrt{\text{eV/amu}}$)	d_γ ($\sqrt{\text{eV/amu}}$)
12	48	0.12	0.48

Table 2: Parameter space for the (10,10) armchair nanotube. Coefficients used for the proportional damping elements are given by d_V, d_Ω, d_K, and d_γ.

The simulation units used are in large part chosen to correspond with atomic-scaled units. Lengths are expressed in Angstroms (1 Å = 1×10^{-10} meters) while forces are expressed as electron volts per Angstrom (eV/Å; 1 eV = 1.60217646 × 10^{-19} Newton-meter). Mass is expressed in terms of atomic mass units (1 amu = 1.660 538 73 × 10^{-27} kilogram). As a result of these choices, the time unit is determined to be Å$\sqrt{\text{amu/eV}}$ which is equivalent to 1.018×10^{-14} seconds, or approximately one one-hundredth of a picosecond. Heretofore, the unit of time measure Å$\sqrt{\text{amu/eV}}$ will simply be referred to as the time unit.

The first computed results given in Fig. 3 illustrate bending response of the (10,10) armchair nanotube loaded at the ends by equal and opposing bending moments in the $\boldsymbol{B}_3$ direction. No inner displacements are computed during the simulation and hence the results are termed unrelaxed. The center node (global node 4) is constrained to have zero velocities (rectilinear and angular) to prevent drifting of the solution. The moments are ramped up linearly in time from zero to their final value of 35 eV at time 1.5×10^4 units. Damping is such that the simulation proceeds nearly quasi-statically to its final equilibrium configuration. Note that all damping coefficients are ramped down to zero in a quadratic manner beginning at time 3.5×10^4 units and ending at time 5×10^4 units.

[2] The special lumped massing technique preserves the relative mass ratios of the diagonal terms in the consistent mass matrix, and also conserves the total mass. Note that the "mass matrix" associated with (25c, 25d) is not a real mass matrix – however, the same lumping technique is used with these equations.

[3] This damping isn't strictly nonconservative since the absolute direction of $\boldsymbol{B}_i$ varies from node to node in the deformed configuration.

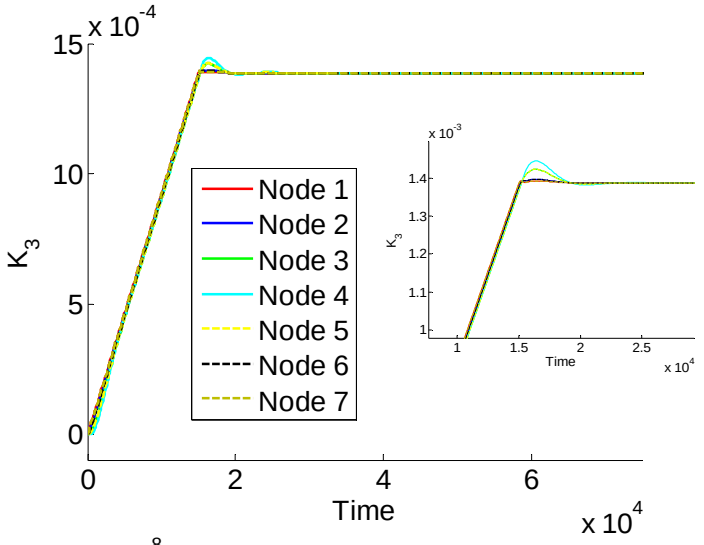

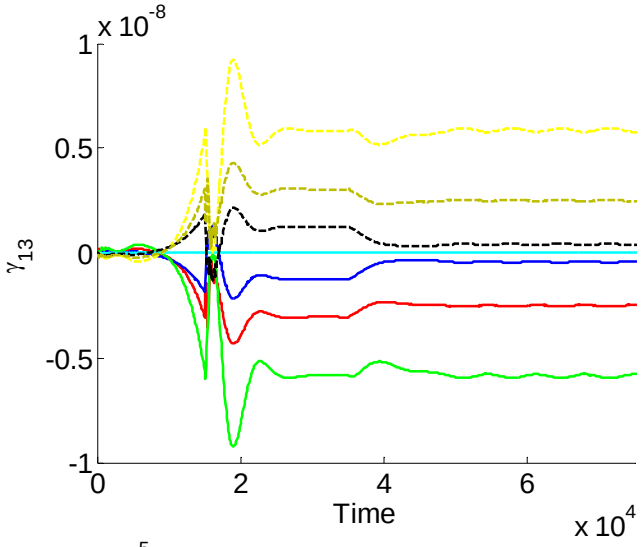

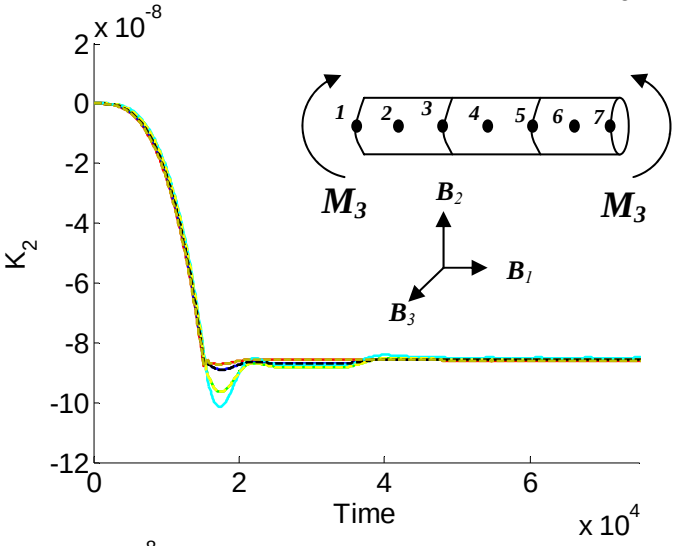

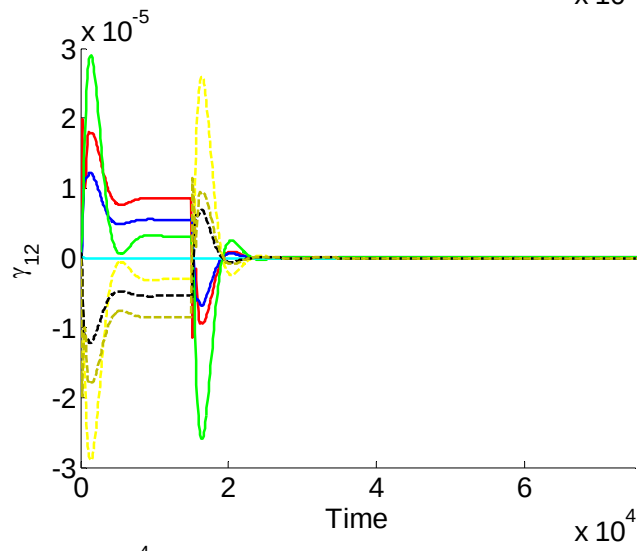

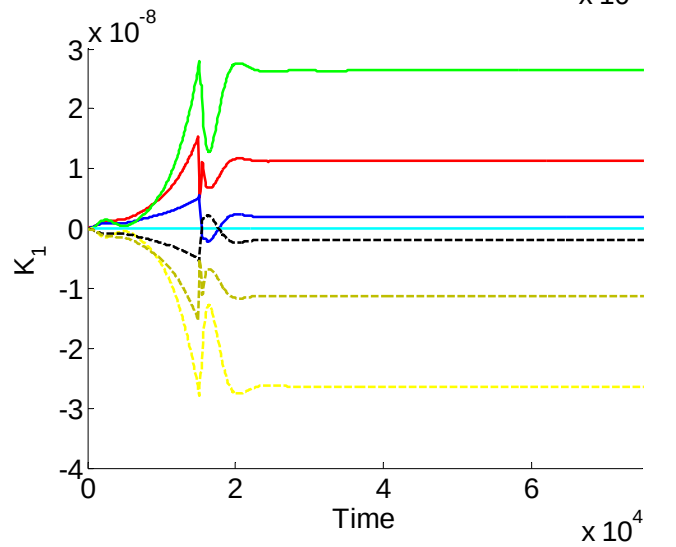

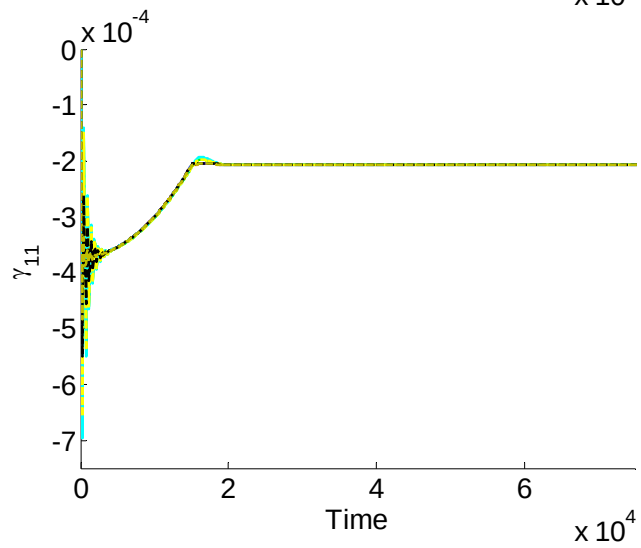

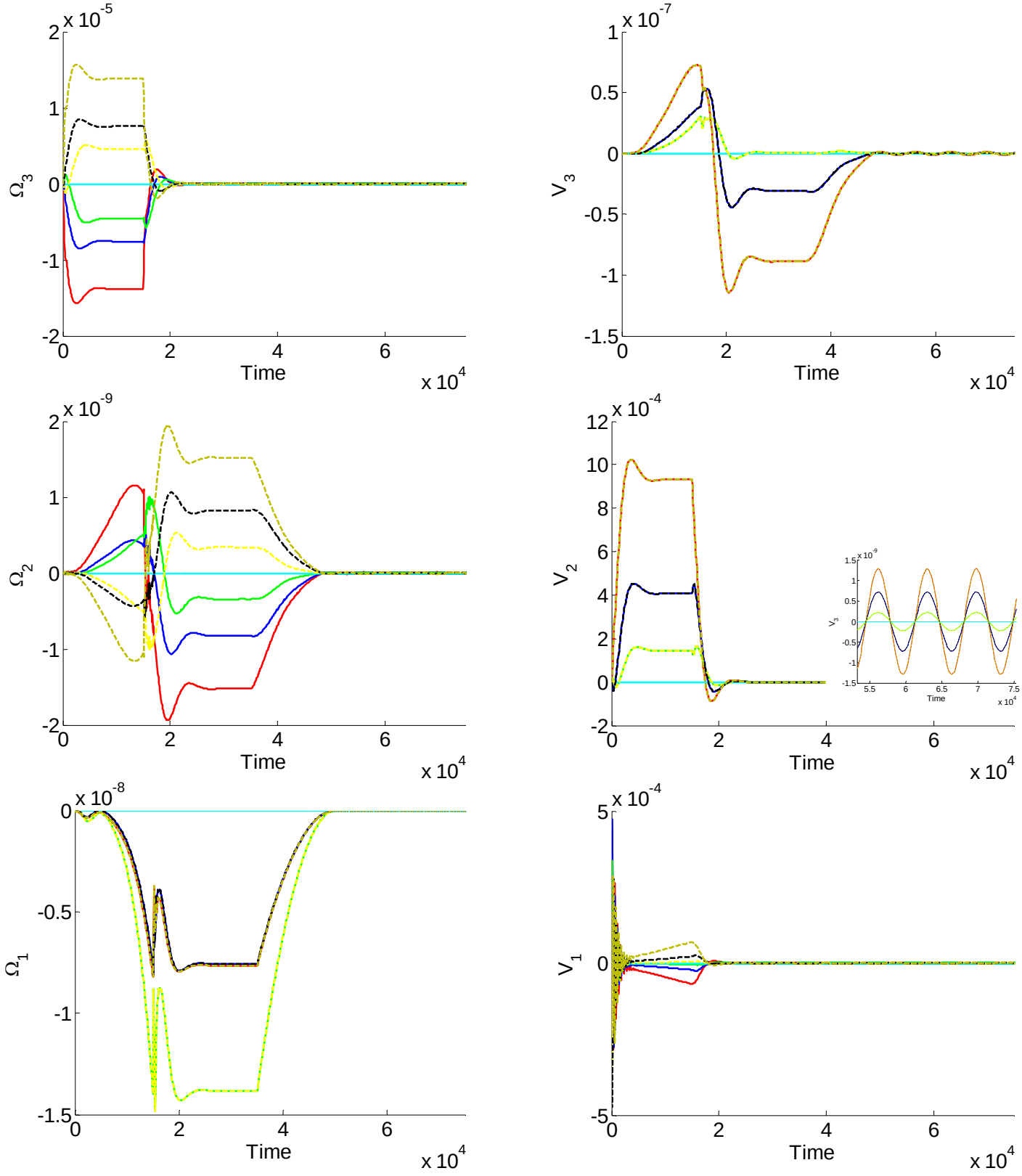

Figure 3: Bending response of the (10,10) armchair nanotube without lattice relaxation.

For completeness, all state time-histories (twelve in total) are presented in Fig. 3. Of interest specifically is the third curvature component time-history given in the first sub-figure. The nanotube's equilibrium curvature of 13.8 $\mathring{A}^{-1}$ results in a substantial angle of bending of roughly 24 degrees. From this result, an average nanotube bending stiffness can be calculated

as M_3 / K_3 = (35 eV) / (13.8×10^{-4} Å^{-1}) = 2.53 eV-μm. For comparison, an approximate bending stiffness of 2.60 eV-μm can be calculated using the elastic theory of beam bending [Srivastava *et al*., 2003]. The bending expression from this theory is $Yh\pi r^3$ where Y is Young's Modulus (taken as 1.2 TPa), h is the van der Waal radius of a single carbon atom (3.4 Å), and r is the (10,10) nanotube radius (6.875 Å). Note that the two bending stiffness values compare favorably and serve as a first verification of the presented formulation. A comparison can also be made with a simulation in which lattice relaxation is performed using inner displacements. Results for the third component of curvature are given in Fig. 4 when inner displacements are calculated every one-hundred time steps. Notice that the predicted equilibrium curvature is now 15.5 Å^{-1} leading to a bending stiffness of 2.3 eV-μm, which as expected, is lower than that calculated without relaxation**.** For small deformations, the added numerical instabilities (as evident in the high frequency content of Fig. 4) associated with a relaxation step, and hence an abrupt system stiffness change, must be weighed versus the incremental change in the system response. As a final remark, the only other deformation state variable of significance is the axial strain γ_{11}, whose time-history demonstrates a residual value at equilibrium of -0.02%. This residual strain is also present in simulations where the loading is absent, and indicates that the initial configuration used (dictated by the initial bond lengths [1.39 Å], bond angles [π/3 rads], and tube radius [6.875 Å]) closely, but not exactly, approximates the actual unloaded equilibrium configuration.

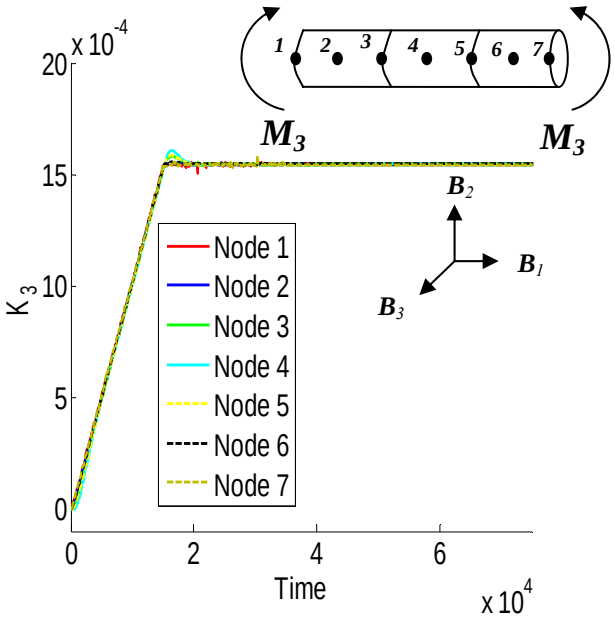

Figure 4: Bending response of the (10,10) armchair nanotube with lattice relaxation.

A second illustration of the damped response of the same (10,10) armchair nanotube (without relaxation) is given in Fig. 5a in which the axial strain time-history is shown for an applied end force of 30 eV/Å in the $\boldsymbol{B}_1$ at global node 7. In this simulation, global node 1 is held fixed by enforcing zero values for its rectilinear and angular velocities. In all other respects, the simulated nanotube and its loading and damping are identical to that used to compute the bending response. As evident in Fig. 5a, the equilibrium axial strain is computed to be 3.11%. This value can be used to calculate an equivalent Young's Modulus when the cross-sectional area is taken to be that of an annular region in which the outer radius is the 6.875 Å and the inner radius differs by the van der Waal radius of a single carbon atom (3.4 Å). The calculation for the Young's Modulus then yields a value of 1.4 TPa, which is well within the reasonable range of values calculated by several previous methods [Srivastava *et al*., 2003; Zhang *et al*., 2004]. Note that if lattice relaxation is performed (Fig. 5b), the computed Young's Modulus drops to 1.3 TPa.

A final illustration of the damped (10,10) armchair's response to loading is given in Fig. 6 in which time-histories for unrelaxed and relaxed lattices are carried out for a twisting moment simulation (35 eV in the $\boldsymbol{B}_1$ direction applied at node 7). The boundary conditions employed are the same as in the axial extension simulation. For the unrelaxed lattice, the equilibrium axial curvature is computed to be 1.76×10^{-3} Å^{-1} while the equilibrium axial curvature for the relaxed lattice is computed to be 2.37×10^{-3} Å^{-1}. This results in predicted average torsional stiffnesses of 1.99 eV-μm and 1.48 eV-μm, respectively. For a comparison, elastic beam theory predicts an approximate torsional stiffness of 1.3 eV-μm computed from the expression $G(2\pi h)r^3$ where G is the shear modulus (taken as 0.30 TPa [Srivastava *et al*., 2003]). Reasonable agreement between a result predicted in this study and an approximate one predicted by a simplified continuum model can again be documented.

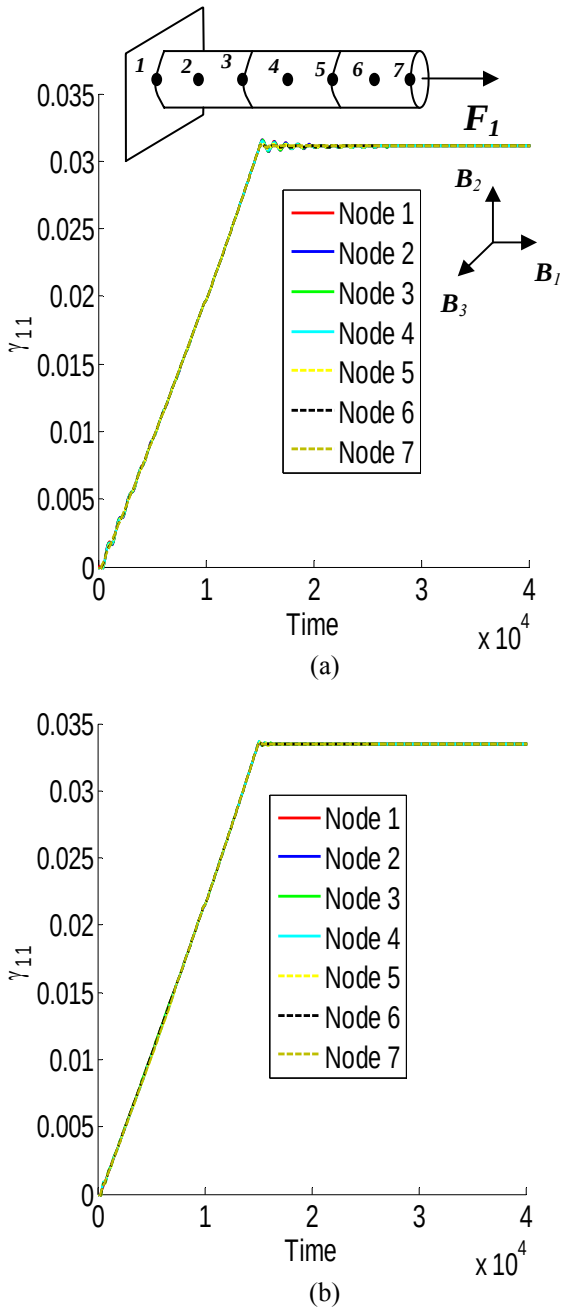

Figure 5: Axial extension of the (10,10) armchair nanotube (a) without lattice relaxation and (b) with lattice relaxation.

7. CONCLUSIONS

An anisotropic beam formulation has been presented for efficient reduced-order modeling of carbon nanotubes in which the intrinsic deformation metrics are taken as curvatures and strains. The material constitutive modeling is derived directly from an atomistic potential and a four-atom representative volume element. An explicit, dynamic finite element framework has also been developed which can be used to simulate the dynamic response of a nanotube to external loading. The resulting computational model has a number of advantages over other continuum and MD formulations, including low-order interpolation functions which describe generally curved and twisted nanotube centerlines using a small number of degrees of freedom; absence of finite rotational variables; and matching of inter-element displacements, slopes, and curvatures at the element boundaries. The equilibrium configuration of an example carbon nanotube in response to bending, axial extension, and torsional loading has been computed and compared to known results in the literature, with good agreement documented in all cases. It is anticipated that the efficiency of the presented nanotube finite element will allow for its use in a more general framework for analyzing nanocomposites where large quantities of nanotube fibers must be simulated together with a matrix material.

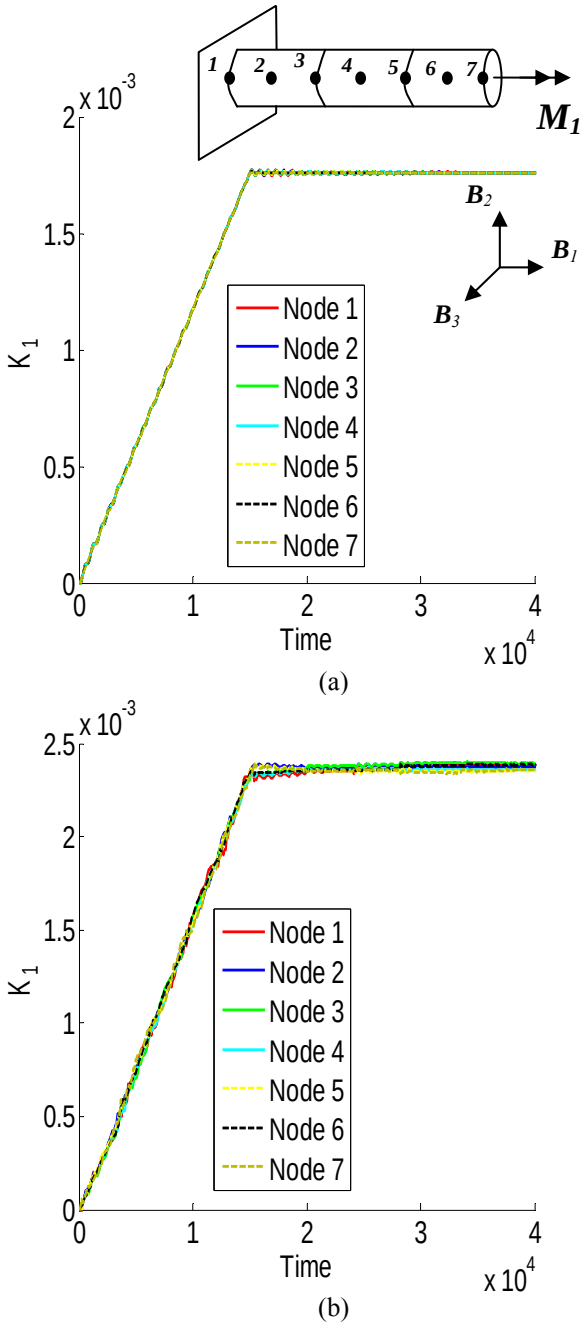

Figure 6: Axial rotation of the (10,10) armchair nanotube (a) without lattice relaxation and (b) with lattice relaxation.

ACKNOWLEDGEMENTS

This work was performed independent of MITRE-sponsored research or sponsor-funded programs, however it has benefited from discussions with Dr. Alfred Brandstein and Dr. Ming-Pin Wang, both of the MITRE Corporation. The author also gratefully acknowledges early nanomechanics discussions with Dr. Peter Chung and Dr. Raju Namburu of the Army Research Labs, Aberdeen, MD.

REFERENCES

[1] Abraham, F., Broughton, J., Bernstein, N., Kaxiras, E., 1998, "Spanning the continuum to quantum length scales in a dynamic simulation of brittle fracture," *Europhys. Lett.,* V. 44, pp. 783–787.

[2] Arroyo, M., Belytschko, T., 2003, "A finite deformation membrane based on inter-atomic potentials for the transverse mechanics of nanotubes," *Mechanics of Materials*, V. 35, pp. 193-215.

[3] Belytschko, T., Xiao, S.P., Schatz, G.C., Ruogg, R.S., 2002, "Atomistic simulations of nanotube fracture," *Physical Review B*, V. 65, 235430.

[4] Belytschko, T., Xiao, S.P., 2003, "Coupling methods for continuum model with molecular model," *J. Mult. Comput. Engrg.,* V. 1, pp. 115–126.

[5] Brenner, D.W., 1990, "Empirical potential for hydrocarbons for use in simulating the chemical vapor deposition of diamond films," *Physical Review B*, V. 42 (15), pp. 9458-9471.

[6] Chung, P.W., Namburu, R. R., 2003, "On a formulation for a multiscale atomistic-continuum homogenization method," *Int. Jour. Of Solids and Structures*, V. 40, pp. 2563-2588.

[7] do Carmo, M. P., 1976, "Differential geometry of curves and surfaces," *Prentice-Hall*, Englewood Cliffs, NJ, USA.

[8] Harris, Peter J. F., 1999, "Carbon nanotubes and related structures," *Cambridge University Press*, Cambridge, UK.

[9] Hernandez, E., Goze, C., Bernier, P., Rubio, A., 1998, "Elastic properties of C and BxCyNz composite nanotubes," *Physical Review Letters,* V. 80, pp. 4502–4505.

[10] Hodges, D.H., 2003, "Geometrically-exact, intrinsic theory for dynamics of curved and twisted, anisotropic beams," *AIAA Journal*, V. 41 (6), pp. 1131-1137.

[11] Hodges, D.H., 1990, "A mixed variational formulation based on exact intrinsic equations for dynamics of moving beams," *Inernational Journal of Solids and Structures*, V. 26 (11), pp. 1253-1273.

[12] Hughes, T.J.R., 1987, "The Finite Element Method – Linear Static and Dynamic Finite Element Analysis," *Prentice-Hall*.

[13] Iijima, S., Brabec, C., Maiti, A., Bernholc, J., 1996, "Structural flexibility of carbon nanotubes.," *Journal of Chemical Physics*, V. 104, pp. 2089–2092.

[14] Li, C., Chou, T-W, 2003, "A structural mechanics approach for the analysis of carbon nanotubes," International Journal of Solids and Structures, V. 40, pp. 2487-2499.

[15] Liu, B., Huang, Y., Jiang, H., Qu, S., Hwang, K.C., 2004, "The atomic-scale finite element method," *Computer Methods in Applied Mechanics and Engineering*, V. 193, pp. 1849-1864.

[16] Odegard, G.M., Gates, T.S., Nicholson, L.M., Wise, K.E., 2002, "Equivalent-continuum modeling of nanostructured materials," *Composites Science and Technology*, V. 62, pp. 1869-1880.

[17] Pantano, A., Parks, D.M., Boyce, M.C., "Mechanics of deformation of single- and multi-wall carbon nanotubes," *Journal of the Mechanics and Physics of Solids*, V. 52, 789-821.

[18] Qian, D., Wagner, G. J., Liu, W. K., Yu, M. F., and Ruoff, R. S., 2002, ''Mechanics of Carbon Nanotubes,'' *Appied Mechanics Reviews*, V. 55, pp. 495–533.

[19] Rudd, R.E., and Broughton, J.Q., 1998, "Coarse-grained molecular dynamics and the atomic limit of finite elements," *Physical Review B*, V. 58 (10).

[20] Srivastava, D., Wei, C., Kyeongjae, C., 2003, "Nanomechanics of carbon nanotubes and composites," *Applied Mechanics Reviews*, V. 56 (2), pp. 215-230.

[21] Tadmor, E. B., Ortiz, M., and Phillips, R., 1996, ''Quasicontinuum analysis of defects in solids,'' *Philos. Mag. A*, V. 73, pp. 1529–1563.

[22] Tadmor, E.B., Smith, G.S., Bernstein, N., Kaxiras, E., 1999, "Mixed finite element and atomistic formulation for complex crystals," *Physical Reivew B*, V. 59 (1), pp. 235-245.

[23] Yakobson, B.I., Campbell, M.P., Brabec, C.J., Bernholc, J., 1997, "High strain rate fracture and C-chain unraveling in carbon nanotubes," *Computational Materials Science,* V. 8, pp. 341–348.

[24] Zanzotto, Giovanni, 1992, "On the material symmetry group of elastic crystals and the Born rule," Arch Rational Mech Anal, 121, pp. 1—36.

[25] Zhang, P., Huang, Y., Gao, H., Hwang, K.C., 2002, "Fracture nucleation in single-wall carbon nanotubes under tension: a continuum analysis incorporating interatomic potentials," *Journal of Applied Mechanics*, V. 69, July, pp. 454-458.

[26] Zhang, P., Jiang, H., Huang, Y., Geubelle, P.H., Hwang, K.C., 2004, "An atomistic-based continuum theory for carbon nanotubes: analysis of fracture nucleation," *Journal of the Mechanics and Physics of Solids*, V. 52, pp. 977-998.